Landau model for the phase diagrams of the orthorhombic rare-earth manganites $R\mathrm{MnO_3}$ (R=Eu, Gd, Tb, Dy, Ho)

J. L. Ribeiro and L. G. Vieira
Centro de Física, Universidade do Minho, 4710-057 Braga, Portugal
(Received 7 April 2010; revised manuscript received 26 May 2010; published 11 August 2010)

The present work aims to describe, within a single phenomenological approach, the specific sequence of phase transitions observed in the rare-earth manganites $R\mathrm{MnO_3}$ at zero magnetic field. It is shown that a single integrated description of the temperature versus composition phase diagrams of these compounds and related solid solutions can be obtained within the scope of Landau theory by adopting the so-called type-II description of the modulated phases.

DOI: 10.1103/PhysRevB.82.064410 PACS number(s): 75.85.+t, 64.70.Rh, 75.47.Lx, 77.80.−e

I. INTRODUCTION

The Landau theory of phase transitions constitutes a powerful tool to describe a great variety of phase transitions and, in particular, phase transitions involving modulated phases. The advantage of this phenomenological approach lies in its ability to establish a direct and exact relationship between the crystal symmetry and the physical properties of the system.[1] By establishing such a relationship, the theory allows us to describe the behavior of macroscopic quantities (such as the polarization, magnetization, dielectric constant, etc.) and to interpret the observed anisotropy or the relevant coupling mechanisms within one exact and symmetry-based framework.

Over the last few years, a great deal of attention has been paid to several metal compounds in which ferroelectricity is induced by a transition to a complex magnetic state.[2–10] In this class of systems, external magnetic fields or chemical pressure fields originated from the partial substitution of a molecular unit are capable of rotating or stabilizing an electrical polarization.[11–17] Although these effects might mimic single phase effects like ferromagnetoelectricity (the linear magnetoelectric effect) or piezoelectricity, they result from rather different mechanisms. Here, the magnetic or the stress fields induce magnetic phase transitions which, in turn, alter the symmetry of the system and modify the set of compatible secondary order parameters. It is from this modification of the symmetry that the change in the polar state of the system originates. Therefore, in this class of compounds, the remarkable cross effects between magnetic ordering and electric polarization relate essentially to the field of improper ferroelectricity.

Among this novel class of compounds, the orthorhombic manganites $R\mathrm{MnO_3}$ (R=Eu, Gd, Tb, Dy, Ho) and related solid solutions such as $\mathrm{Eu_{1-x}Y_xMnO_3}$, $\mathrm{Gd_{1-x}Tb_xMnO_3}$, or $\mathrm{Dy_{1-x}Tb_xMnO_3}$ are those possessing the simplest crystallographic and magnetic structures. Because of this reason, these compounds constitute adequate model systems in which symmetry-based models can be explored. The present work takes advantage of this fact to obtain, for these compounds, a single integrated model capable of accounting for the observed sequence of phase transitions. As it will be shown, this integrated picture can be obtained within the scope of the so-called type-II Landau description of the modulated phases[18] and can be used to interpret, model, and organize the experimental data concerning the temperature versus composition phase diagrams of the pure compounds and of their solid solutions.

Landau models based on homogeneous magnetic order parameters have been previously used to analyze the phase transitions observed in several $\mathrm{LaMnO_3}$-based rare-earth systems. For example, the noncollinear magnetic structure of $\mathrm{LaMnO_3}$ in an external magnetic field has been investigated on the basis of a free-energy expansion in terms of the different manganese spin basis modes.[19] A similar approach has also been used to analyze the symmetry changes in the paramagnetic (PM) to A-type antiferromagnetic (AFM) and to ferromagnetic phase transitions in undoped and moderately doped $\mathrm{LaMnO_3}$ (Ref. 20). However, in these previous works, the stabilization of modulated spin phases or the induction of improper ferroic properties have not been addressed.

It should also be mentioned that the present study focus essentially on insulating systems that are either pure rare-earth compounds or mixed solid solutions of isoelectric ions. In many manganese perovskites with a colossal magnetoresistence, charge-density waves may eventually coexist with spin modulations. This coexistence and interaction of two different types of order parameters can be analyzed within the framework of Landau theory.[21] However, because the charge-density waves observed in these systems originate essentially from the partial replacement of the trivalent rare-earth ions by divalent alkaline-earth ions ($R^{3+}_{1-x}AE^{2+}_x\mathrm{MnO_3}$) we will not consider this type of order parameter. Hence, we will focus here on pure magnetic spin modulated phases even if the subtle coupling between lattice, spin, charge, and orbital degrees of freedom may still challenge our understanding of this type of oxides.

II. PHASE TRANSITIONS IN THE DIFFERENT $R\mathrm{MnO_3}$ COMPOUNDS

At room temperature, the symmetry of the orthorhombic rare-earth manganites $R\mathrm{MnO_3}$ is described by the paramagnetic group $G=(Pnma)'$ and the unit-cell possesses four molecular formulas (Z=4).[22] The magnetic phases observed at lower temperatures result essentially from the ordering of the Mn spins $\vec{S}_1$, $\vec{S}_2$, $\vec{S}_3$, and $\vec{S}_4$ which, in the paramagnetic phase,

TABLE I. Possible magnetic basis modes originated from the Mn^{3+} located in 4*b* Wyckoff positions.

$A_g^-(\Delta_1)$	$B_{2g}^-(\Delta_2)$	$B_{3g}^-(\Delta_3)$	$B_{1g}^-(\Delta_4)$
G_x	F_y	F_x	F_z
A_z	A_x	A_y	G_y
C_y	G_z	C_z	C_x

are located in the unit cell at the positions (0,0, $\frac{1}{2}$), ($\frac{1}{2}$,0,0), (0, $\frac{1}{2}$, $\frac{1}{2}$), and ($\frac{1}{2}$, $\frac{1}{2}$, 0), respectively. The spins of the rare-earth ion may eventually play a role, especially at lower temperatures, but we will ignore their contribution because they are not essential for the understanding of the global phase diagrams observed.

At the center of the Brillouin zone ($\vec{k}=0$), the 12 components of the Mn spins generate a reducible corepresentation Γ of the paramagnetic space group, whose decomposition into a direct sum of irreducible corepresentations leads to $\Gamma=3A_g^- \oplus 3B_{1g}^- \oplus 3B_{2g}^- \oplus 3B_{3g}^-$. Here, the (−) superscript signals the odd character of these corepresentations under time reversal. To each irreducible corepresentation there will correspond a set of magnetic basis modes, as specified in Table I.

In this table, the basis modes are denoted as $\vec{A}=\vec{S}_1+\vec{S}_2-\vec{S}_3-\vec{S}_4$, $\vec{G}=\vec{S}_1-\vec{S}_2-\vec{S}_3+\vec{S}_4$, $\vec{F}=\vec{S}_1+\vec{S}_2+\vec{S}_3+\vec{S}_4$, and $\vec{C}=\vec{S}_1-\vec{S}_2+\vec{S}_3-\vec{S}_4$. This notation directly specifies the relative orientation of the different spins.[12] For example, for the mode $\vec{A}$, the spins pairs ($\vec{S}_1$,$\vec{S}_2$) and ($\vec{S}_3$,$\vec{S}_4$) are oriented parallel to each other within each set and both sets are antiferromagnetically coupled.

As in the prototype case of $LaMnO_3$ (Ref. 22), the Mn^{3+} electronic configuration is $t_{2g}^3 e_g^1$, with the spin quantum number $S=2$. The three t_{2g}^3 electrons are localized while the e_g electron orbitals are extended in the basal (010) plane[23] and are strongly hybridized with the oxygen *p* orbitals. The ferromagnetic superexchange interactions of the e_g^1 electrons in the (010) plane and the antiferromagnetic interactions of the t_{2g}^3 electrons out of the plane favor the onset, at low temperatures, of one antiferromagnetic order of the *A* type (*A* AFM). This is well apparent in the set of systems ranging from La to Sm, where a direct transition from the PM phase to one *A*-AFM phase is observed. Here, the AFM order results precisely from the stabilization of the A_x irreducible magnetic mode (see Table I). Consequently, the system acquires a symmetry described by the magnetic space group $Pnma(P1\frac{2_1}{m}1)$ (Ref. 24) and a canted ferromagnetic moment directed along the $\vec{b}$ axis.

However, smaller rare-earth ions (Eu^{3+}, Gd^{3+} Tb^{3+}, Y^{3+}, etc.) fit worse in the perovskite network and give rise to more pronounced *b*-axis rotations of the Mn-O octahedra. The Mn-O-Mn bonding angles diminish and the orthorhombic distortion of the lattice increases as the ionic radius is reduced.[25] This effect weakens the in-plane ferromagnetic superexchange interactions and modifies the orbital overlap and the relative strength of the antiferromagnetic interaction between the next-nearest neighbors Mn^{3+} spins. The ferromagnetic order of the in-plane spins tends to become strongly frustrated.

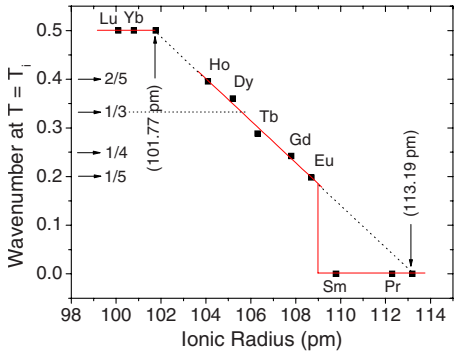

FIG. 1. (Color online) The ionic radius of the rare-earth elements (from Pr to Lu) plotted as a function of the modulation wave number immediately below the stability limit of the paramagnetic phase. The straight line from Ho to Eu is a linear fit. The points marked by arrows at the ionic radii 101.77 and 113.19 pm were obtained by extrapolation of that best fit.

At first, this geometrically driven effect simply decreases the Néel temperature from 140 K (La) to 60 K (Sm). However, beyond a certain threshold and within the range delimited by Eu and Ho, the magnetic instability shifts from the center to the interior of the Brillouin zone (along the Σ line), giving rise to an intermediate longitudinal incommensurate (L-INC) phase, with a modulation wave vector $\vec{k}=\delta(T)\vec{a}^*$ (Refs. 25–28). The corresponding incommensurate order parameter is still irreducible and of the symmetry $\Gamma(B_2)$ (Refs. 4 and 29–31; see notation in Ref. 32), containing therefore the active mode A_x in the limit $\vec{k}\to 0$ $[\lim_{\vec{k}\to 0}\Gamma(B_2)=B_{2g}^- \oplus B_{1u}^+]$. Given the one-to-one relationship existing in this case between each of the irreducible corepresentations of the paramagnetic group and the symmetry of the corresponding modulated phase,[33] this L-INC phase must have the symmetry described by the magnetic superspace group $P_a(P_{11S}^{nma})$ (Ref. 34). This symmetry is incompatible with any ferroic or linear magnetoelectric properties.

Figure 1 shows the value of the modulation wave number observed immediately below the transition from the PM phase, $\delta(T_i)$, as a function of the ionic radius R_{ion} of the rare-earth element (data taken from Ref. 25). As seen, the L-INC phase sets in at a location in the Brillouin zone that varies linearly with R_{ion}. Therefore, the instability of the PM phase moves along a single magnon branch, approaching the Brillouin-zone boundary (*X* point, $\delta=1/2$) as R_{ion} decreases (see also Ref. 35). This drift of $\delta(T_i)$ can be extrapolated in the direction of larger or smaller values of R_{ion}. This extrapolation indicates that the center and the border of the Brillouin zone would be reached for R_{ion} on the order of 113 pm and 102 pm, respectively. This latter value is very close to the ionic radius of both Yb^{3+} and Lu^{3+} (100.8 pm and 100.1 pm, respectively), for which the orthorhombic $RMnO_3$ system shows direct transitions from the paramagnetic phase to one *E*-type antiferromagnetic (*E*-AFM) phase[36] (Refs. 35 and 37–40). The observed *E*-AFM order consists of [101] rows of spins coupling parallel to a neighboring row on one side and antiparallel on the other with an antiparallel coupling between (010) planes. This spin structure corresponds to the one expected for the lock in of one order parameter of sym-

metry $\Gamma(B_2)$ at the Brillouin-zone edge $\vec{k}=\frac{1}{2}\vec{a}^*$ (Ref. 39), for a global phase $\Phi=\pi/4$ (Ref. 33). The corresponding magnetic group is $P_a(Pnm2_1)$ and a ferroelectric polarization directed along the c axis is then allowed by symmetry.[32] This polarization is actually observed in the E-AFM phase of $HoMnO_3$, $YbMnO_3$, or $LuMnO_3$ (Refs. 16 and 41) (as well as in the E-AFM phase of some nickelates[42–45]). It provides one striking example of improper ferroelectricity driven by an irreducible and colinear magnetic order parameter. In contrast to the most extensively theoretically studied case of spiral magnetism, the mechanism responsible for the polar order does not rely here on the presence of an anisotropic Dzyaloshinsky-Moriya interaction[46,47] (see also Ref. 16) and cannot be accounted for by the models designed for noncollinear magnets such as the spin current model,[48] the electric current cancellation model,[49] or by the usual heuristic pictures.[50]

The above observations can be summarized by saying that, over the whole set of orthomanganese compounds, the primary instability of the paramagnetic phase moves from the center to the edge of the Brillouin zone along a single magnon branch of symmetry $\Gamma(B_2)$. This common symmetry of the primary order parameter will be essential for our present purposes. However, one additional question concerning the possible role of other (secondary) magnetic distortions must be analyzed in order to elucidate the relevant set of magnetic order parameters. Let us first notice that, in systems such as $TbMnO_3$ or $DyMnO_3$, there occur, at lower temperatures, cycloidal phases resulting from the stabilization of order parameters of symmetry $\Gamma(B_2)+\Gamma(A_2)$ (at zero magnetic field) or, in the case of $TbMnO_3$, $\Gamma(B_2)+\Gamma(A_1)$ under magnetic fields.[29,51] Besides the primary branch $\Gamma(B_2)$, the additional branches involved here have symmetries $\Gamma(A_2)$ and $\Gamma(A_1)$. These branches correspond to spatial modulations of the magnetic modes A_y and A_z given in Table I [$\lim_{\vec{k}\to 0}\Gamma(A_2)=B_{3g}^-\oplus A_u^+$ and $\lim_{\vec{k}\to 0}\Gamma(A_1)=A_g^-\oplus B_{3u}^+$]. Also, in orthorhombic $HoMnO_3$, for example, the observed diffraction patterns correspond to parent reflections (hkl) satisfying $h+l=2n$ and $k=2n+1$ (n integer).[35] Given that the Mn^{3+} ions occupy, in the paramagnetic unit cell, $4b$ Wyckoff sites, the observed reflection conditions imply that the spin wave can only include A modes. Hence, even if the A_x mode may be seen as primary, all the three A modes seem to play a role in the phase-transition sequences observed in the $RMnO_3$ system. Other nonmagnetic secondary order parameters that are allowed by the symmetry must also be taken into account.

III. LANDAU FREE ENERGY

In the usual Landau theoretical framework for incommensurate systems, both the lock-in commensurate phase (either homogeneous or modulated) and the incommensurate phase are described by a common primary order parameter: the symmetry of the primary distortion is kept invariant while the modulation wave vector changes with temperature, composition or external fields.[1] In the case of the orthorhombic rare-earth manganites $RMnO_3$, the modulation wave vector is kept fixed along a main crystallographic direction ($\vec{k}=\delta\vec{a}^*$) and, as seen in the preceding section, the primary order parameter maintains its symmetry $\Gamma(B_2)$, over the entire range of the rare-earth elements. It is this common symmetry of the primary parameter over the whole set of compounds that allows us to deal with the different systems within one unified model.

One incommensurate phase is normally seen as a modulation or a periodic distortion of a given underlying commensurate or lock-in phase. The dimension of the incommensurate order parameter will therefore depend on the dimension of the basic commensurate order parameter chosen for the description. For the case in hands, if the lock-in wave vector is located inside the Brillouin zone, then the commensurate order parameter is a complex number representing the amplitude of the magnetic wave and its global phase with respect to the underlying lattice. The incommensurate modulation (the distortion of the lock-in phase) is here stabilized by a Lifshitz invariant[52] and the evolution of the wave number toward its lock-in value originates from the competition between this term and the umklapp potentials favoring the commensurate order. This case corresponds to the so-called type-I description of an incommensurate phase.[18] In the case of the rare-earth manganites, this type of description has been previously used to elucidate the relationship between the symmetry of a given modulated magnetic phase, either commensurate or incommensurate, and the primary ferroic properties.[32]

If, on the other hand, the lock-in phase is taken as homogeneous ($\vec{k}=0$) then, for the symmetry here considered, the order parameter is necessarily one dimensional and the Lifshitz invariant forbidden. In such a case, the stabilization of a modulated spin structure may only be obtained by considering a free-energy density expansion containing invariants which depend on the spatial derivatives of the one-dimensional primary order parameter. This second description of a modulated incommensurate phase is called of the type II.[18] It is far more versatile if one wants to go beyond the description of a particular phase transition and capture, within a single phenomenological model, a sequence of phase transitions, a temperature versus magnetic field, or a temperature versus composition phase diagram involving a single critical branch. This versatility has been well demonstrated in the case of displacive systems such as sodium nitrite,[53] thiourea,[54] or betaine calcium chloride dihydrate (BCCD) (Ref. 55) and, with the necessary adaptations, can be used for the case of the $RMnO_3$ compounds.

A. Landau free-energy density

Let us then consider the problem of finding the adequate type-II free-energy density expansion. For the chosen lock-in wave vector ($\vec{k}=0$), the primary order parameter is the A_x magnetic mode. In order to accommodate the possible stabilization of a modulated spin structure, the free-energy density must include terms depending on the spatial derivatives of this mode. The symmetry constraints that are verified here correspond exactly to those that are observed in displacive systems such as $NaNO_2$, $SC(NH_2)_2$, or BCCD.[53–55] Consequently, similar to these systems, this part of the free-energy density can be written as

$$f_1 = \frac{1}{2}\alpha_x A_x^2 + \frac{1}{4}\beta_x A_x^4 - \frac{1}{2}\sigma\left(\frac{\partial A_x}{\partial X}\right)^2 + \frac{1}{4}\gamma\left(\frac{\partial^2 A_x}{\partial X^2}\right)^2 + \nu A_x^2\left(\frac{\partial A_x}{\partial X}\right)^2. \quad (1)$$

The dispersive term $\nu A_x^2(\frac{\partial A_x}{\partial X})^2$ is symmetry allowed because it is the product of two trivial invariants. It is this term that imposes the temperature dependence of the modulation wave vector, favoring energetically smaller or higher values of the modulation wave vector if $\nu>0$ or $\nu<0$, respectively. Negative $(-\sigma)$ and positive (γ) coefficients must be chosen in order to stabilize a minimum in the dispersion of the quadratic term at an arbitrary point of the Brillouin zone, a necessary condition for the occurrence of modulated spin structures. As usual, we will take $\alpha_x=\alpha_{0x}(T-T_0)$ with $\alpha_{0x}>0$ and $\beta_x>0$.[56]

In the case of the secondary magnetic order parameters A_y and A_z, we will adopt the simplest possible free energy density, limiting the expansion to terms up to the fourth order. Also, the biquadratic mixed terms $A_x^2A_y^2$ and $A_x^2A_z^2$ will be considered to describe the coupling between the primary and the secondary magnetic order parameters. Consequently, we have

$$f_2 = \frac{1}{2}\alpha_y A_y^2 + \frac{1}{4}\beta_y A_y^4 + \frac{1}{2}\alpha_z A_z^2 + \frac{1}{4}\beta_z A_z^4 + \Delta_1 A_x^2 A_y^2 + \eta_1 A_x^2 A_z^2. \quad (2)$$

Here, we will take $\beta_y,\beta_z,\Delta_1,\eta_1>0$ and $\alpha_{y(z)}=\alpha_{y(z)0}(T-T_{1(2)})$, with $T_1<T_0$ and $T_2<T_0$. This latter choice means that we will assume that the secondary magnetic order parameters also possess intrinsic instabilities, although at temperatures lower than T_0. Hence, in the absence of any interaction between the three magnetic order parameters (that is, when $\Delta_1=\eta_1=0$), a sequence of second-order transitions would occur between phases characterized by the order parameters A_x, $A_x\oplus A_y$ (or $A_x\oplus A_z$), and $A_x\oplus A_y\oplus A_z$. The positive sign chosen for Δ_1 and η_1, however, implies the possible suppression of this phase sequence and the first-order character of an eventual transition between any two of these magnetic phases. Notice that for $\Delta_1<0$ and/or $\eta_1<0$, trigger-type phase transitions could occur even without any intrinsic instability of the secondary magnetic order parameters.

In addition to the pure magnetic invariants considered so far, we must also take into account other terms coupling the magnetic degrees of freedom with other secondary parameters. Here, because we are interested in the possibility of improper ferroelectricity or improper ferroelasticity, we will consider the particular case of coupling terms that are linear on one electric polarization or on one homogeneous lattice strain. From the transformation properties of the first spatial derivative of the primary parameter, $\frac{\partial A_x}{\partial x}$ and of products such as $A_y\frac{dA_x}{dx}$, $A_z\frac{dA_x}{dx}$, A_yA_x, and A_yA_x (see Table II), it becomes clear that the polarizations P_y and P_z, [which are transformed, under $(Pnma)'$, as B_{2u}^+ and B_{3u}^+, respectively], along with the lattice deformations e_{xy} and e_{xz} [B_{1g}^+ and B_{2g}^+, respectively] are potential secondary parameters allowed by symmetry. The contribution of these mixed terms to the free-energy density is of the form[57]

TABLE II. Transformation properties of the terms bilinear in the magnetic order parameters or involving the first-order spatial derivative of the primary order parameter.

	C_{2x}	C_{2y}	i	θ	
x	1	−1	−1	1	B_{3u}^+
A_x	−1	1	1	−1	B_{2g}^-
A_y	1	−1	1	−1	B_{3g}^-
A_z	1	1	1	−1	A_g^-
$A_y\frac{dA_x}{dx}$	−1	1	−1	1	B_{2u}^+
A_yA_x	−1	−1	1	1	B_{1g}^+
$A_z\frac{dA_x}{dx}$	−1	−1	−1	1	B_{3u}^+
A_zA_x	−1	1	1	1	B_{2g}^+

$$f_3 = \Delta_2 A_y\left(\frac{\partial A_x}{\partial X}\right)P_y + \Delta_3 A_y A_x e_{xy} + \eta_2 A_z\left(\frac{\partial A_x}{\partial X}\right)P_z + \eta_3 A_z A_x e_{xz} + \frac{P_y^2}{2\chi_y} + \frac{P_z^2}{2\chi_z} + \frac{e_{xy}^2}{2c_{xy}} + \frac{e_{xz}^2}{2c_{xz}}. \quad (3)$$

Notice that, for simplicity, we have neglected invariants involving more than two secondary parameters, such as $P_xP_ye_{xy}$, $P_xP_ze_{xz}$, or $A_yA_ze_{yz}$. This means that we are neglecting the potential stabilization of phases with very low symmetry. Although these phases may play a role in the detailed mechanisms for a given phase transition,[33,58,59] they are not essential for the global picture we pursue here. Also, we are ignoring the eventual commensurate character of the spin wave by not including eventual mixed umklapp terms that are allowed for particular types of commensurate phases.[32,33]

The free-energy density $f=f_1+f_2+f_3$ corresponds to the simplest possible functional with the potential to describe the observed zero-field phase diagrams of the $R\mathrm{MnO_3}$ compounds. However, it still contains an undesirable large number of adjustable constants.

B. Reduced variables and some simplifying assumptions

As usual, the first step to improve the situation regarding the number of model parameters is the elimination of a number of physically irrelevant coupling constants. This can be achieved by expressing the free-energy density in terms of dimensionless quantities. By defining $g=\frac{\gamma^2\beta_x}{16\sigma^4}f$, $A_i=\frac{2\sigma}{(\gamma\beta_x)^{1/2}}S_i$, $X=(\frac{\gamma}{2\sigma})^{1/2}x$, $\frac{\beta_x^{1/2}\gamma}{2\sigma^2\chi_y^{1/2}}P_{y(z)}=p_{y(z)}$, $a_{y(z)}=\frac{\alpha_{y0}(\alpha_{z0})}{\alpha_{x0}}$, $b_{y(z)}=\frac{\beta_y(\beta_z)}{\beta_x}$, $\bar{\chi}_z=\frac{\chi_z}{\chi_y}$, $t=\frac{\gamma}{8\sigma^2}\alpha_{0x}(T-T_0)$, $\beta_x^{-1}\Delta_1(\eta_1)=\nabla_1(\xi_1)$, $\nabla_2(\xi_2)=\Delta_2(\eta_2)[\frac{\chi_y\sigma}{2\beta_x\gamma}]^{1/2}$, and $\nabla_3(\xi_3)=\frac{\gamma}{4\sigma^2}\Delta_3(\eta_3)$, one obtains the simpler reduced free-energy density

$$g(x) = tS_x^2 + \frac{1}{4}S_x^4 - \frac{1}{4}\left(\frac{\partial S_x}{\partial x}\right)^2 + \frac{1}{4}\left(\frac{\partial^2 S_x}{\partial x^2}\right)^2 + \mu S_x^2\left(\frac{\partial S_x}{\partial x}\right)^2 + a_y(t-t_1)S_y^2 + \frac{1}{4}b_y S_y^4 + \nabla_1 S_x^2 S_y^2 + \nabla_2 p_y S_y\left(\frac{\partial S_x}{\partial x}\right) + \nabla_3 S_x S_y e_{xy} + a_z(t-t_2)S_z^2 + \frac{1}{4}b_z S_z^4 + \xi_1 S_x^2 S_z^2 + \xi_2 p_z S_z\left(\frac{\partial S_x}{\partial x}\right) + \xi_3 S_x S_z e_{xz} + \frac{p_y^2}{2} + \frac{p_z^2}{2\bar{\chi}_z} + \frac{e_{xy}^2}{2\bar{c}_{xy}} + \frac{e_{xz}^2}{2\bar{c}_{xz}}. \quad (4)$$

Moreover, we will introduce two additional approximations that will allow us to reduce further the number of the parameters and will help us to simplify the calculations to be made. First, we notice that, for a cubic perovskite, $\bar{\chi}_z = a_y = a_z = b_y = b_z = 1$. Although this is no longer true in the presence of an orthorhombic distortion, it seems reasonable to assume that one can keep these values as a first approximation and eliminate five nonessential adjustable parameters.[60] We will also use a simple plane wave to describe the magnetic modulation induced by the primary order parameter S_x. This second approximation can be justified by noticing that, over the whole temperature range of stability of the observed longitudinal or cycloidal modulated phases, essentially only first-order magnetic satellites are observed in neutron or x-ray measurements. The plane-wave approximation is therefore expected to describe reasonably well the magnetic modulation over the whole temperature and magnetic field ranges explored experimentally. Accordingly, we will write in Eq. (4) $S_x = \sigma_x \cos(qx)$, obtaining

$$g(x) = \left[t\cos^2(qx) - \frac{q^2}{4}\sin^2(qx) + \frac{q^4}{4}\cos^2(qx)\right]\sigma_x^2 + \frac{1}{4}[\cos^4(qx) + 4\mu q^2 \sin^2(qx)\cos^2(qx)]\sigma_x^4 + (t-t_1)S_y^2 + \frac{1}{4}S_y^4 + \nabla_1 S_y^2\sigma_x^2\cos^2(qx) - \nabla_2 S_y q\sigma_x p_y \sin(qx) + \nabla_3 S_y\sigma_x e_{xy}\cos(qx) + (t-t_2)S_z^2 + \frac{1}{4}S_z^4 + \xi_1 S_z^2\sigma_x^2\cos^2(qx) - \xi_2 q S_z\sigma_x p_z \sin(qx) + \xi_3 S_z\sigma_x e_{xz}\cos(qx) + \frac{p_y^2}{2} + \frac{p_z^2}{2} + \frac{e_{xy}^2}{2\bar{c}_{xy}} + \frac{e_{xz}^2}{2\bar{c}_{xz}}. \quad (5)$$

C. Nonmagnetic order parameters

The equilibrium value of a given secondary and nonmagnetic order parameter X (here, as seen, $X = P_y$, P_z, e_{xz}, or e_{xy}) can be determined by imposing in Eq. (5) the condition $\frac{\partial g}{\partial X} = 0$. This leads to the following relations between nonmagnetic and magnetic order parameters:

$$p_y = \nabla_2 q\sigma_x S_y \sin(qx),$$

$$p_z = \xi_2 q\sigma_x S_z \sin(qx),$$

$$e_{xy} = -\bar{c}_{xy}\nabla_3\sigma_x S_y \cos(qx),$$

$$e_{xz} = -\bar{c}_{xz}\xi_3\sigma_x S_z \cos(qx). \quad (6)$$

Notice that, here, the improper polarizations p_z and p_y can only occur in magnetic modulated phases ($q \neq 0$) involving at least two irreducible components of the magnetic modulation (note again that we are ignoring the eventual commensurate nature of the modulation wave vector) while the lattice deformations can be maintained even in the case of a homogeneous phase. By substituting Eq. (6) into Eq. (5) one can then express the free-energy density as a function of the magnetic order parameters,

$$g(x) = \left[t\cos^2(qx) - \frac{q^2}{4}\sin^2(qx) + \frac{q^4}{4}\cos^2(qx)\right]\sigma_x^2 + \frac{1}{4}[\cos^4(qx) + 4\mu q^2 \sin^2(qx)\cos^2(qx)]\sigma_x^4 + (t-t_1)S_y^2 + \frac{1}{4}S_y^4 + \frac{1}{2}gS_y^2\sigma_x^2\cos^2(qx) - \frac{1}{2}\nabla_2^2 q^2 S_y^2\sigma_x^2\sin^2(qx) + (t-t_2)S_z^2 + \frac{1}{4}S_z^4 + \frac{1}{2}hS_z^2\sigma_x^2\cos^2(qx) - \frac{1}{2}\xi_2^2 q^2 S_z^2\sigma_x^2\sin^2(qx). \quad (7)$$

Here, we have defined $g = 2\nabla_1 - \bar{c}_{xy}\nabla_3^2$ and $h = 2\xi_1 - \bar{c}_{xz}\xi_3^2$.

In the free-energy density [Eq. (7)], the order parameter A_x plays a central role not only because it softens at a higher temperature but also because it is the one that gives rise to the spin modulation wave. It is the instability of this primary mode that can trigger the stabilization of a modulation wave of S_y or S_z, whose intrinsic instabilities would otherwise give rise to homogeneous phases. In fact, by imposing in Eq. (7) the conditions $\frac{\partial g(x)}{\partial S_y} = 0$ and $\frac{\partial g(x)}{\partial S_z} = 0$ one readily obtains

$$S_y^2 = \sigma_{yF}^2\cos^2(qx) + \sigma_{yA}^2\sin^2(qx), \quad (8a)$$

$$S_z^2 = \sigma_{zF}^2\cos^2(qx) + \sigma_{zA}^2\sin^2(qx) \quad (8b)$$

with $\sigma_{yF}^2 = -[2(t-t_1) + g\sigma_x^2]$, $\sigma_{yA}^2 = -[2(t-t_1) - \nabla_2^2 q^2\sigma_x^2]$, $\sigma_{zF}^2 = -[2(t-t_2) + h\sigma_x^2]$, and $\sigma_{zA}^2 = -[2(t-t_2) - \xi_2^2 q^2\sigma_x^2]$.

As seen, it is the onset of a longitudinal modulation wave $S_x = \sigma_x \cos(qx)$ that can provoke, via the biquadratic coupling terms between the magnetic parameters, to the modulation wave of the components of S_y or S_z. It is also clear that these secondary magnetic modulations can be mainly established either in phase (σ_{yF} or σ_{zF}) or in quadrature (σ_{yA} or σ_{zA}) with respect to S_x, depending on the values of the coefficients. These two possible sets of components of the secondary magnetic modulation have in fact different symmetries and couple, consequently, to different homogeneous parameters. For example, as we have seen in Eq. (6), $p_y = \nabla_2 q S_y\sigma_x \sin(qx)$ and $e_{xy} = -\bar{c}_{xy}\nabla_3 S_y\sigma_x\cos(qx)$. If, for example, $S_y = \sigma_{yF}\cos(qx)$, then $p_y = \nabla_2 q\sigma_{yF}\sigma_x \sin(qx)\cos(qx)$ and $e_{xy} = -\bar{c}_{xy}\nabla_3\sigma_{yF}\sigma_x\cos^2(qx)$. That is, if S_y is in phase with S_x, the value of the polarization wave, averaged over one

period of the modulation, is null, $\langle p_y \rangle = 0$, while the lattice deformation e_{xy} is not ($\langle e_{xy} \rangle \neq 0$). Conversely, if $S_y = \sigma_{yA} \sin(qx)$, then $\langle p_y \rangle \neq 0$ and $\langle e_{xy} \rangle = 0$. Therefore, the stabilization of an improper polarization $\langle p_y \rangle$ or $\langle p_z \rangle$ requires the stabilization of secondary spin waves S_y or S_z in quadrature with S_x. Notice that, in any case, the secondary spin waves are triggered by the primary order parameter and, consequently, share the same wave vector. All these features are, in fact, observed experimentally.

By replacing Eq. (8) into Eq. (7), one can then express the free-energy density as a function of the new set of magnetic order parameters σ_x, σ_{yF}, σ_{yA}, σ_{zF}, and σ_{zA},

$$\begin{aligned} g(x) = & \left[t\cos^2(qx) - \frac{q^2}{4}\sin^2(qx) + \frac{q^4}{4}\cos^2(qx) \right]\sigma_x^2 \\ & + \frac{1}{4}[\cos^4(qx) + 4\mu q^2 \sin^2(qx)\cos^2(qx)]\sigma_x^4 \\ & - \frac{1}{4}[\sigma_{yF}^2 \cos^2(qx) + \sigma_{yA}^2 \sin^2(qx)]^2 \\ & - \frac{1}{4}[\sigma_{zF}^2 \cos^2(qx) + \sigma_{zA}^2 \sin^2(qx)]^2. \end{aligned} \tag{9}$$

D. Free energy of the competing phases

The general free-energy functional G can now be obtained by averaging [Eq. (9)] over one period of the magnetic modulation $\left[G = \frac{1}{x_0}\int_0^{x_0} g(x)dx\right]$. This leads to

$$\begin{aligned} G = & \frac{1}{2}\left[t - \frac{q^2}{4} + \frac{q^4}{4} \right]\sigma_x^2 + \frac{1}{4}\left[\frac{3}{8} + \frac{\mu q^2}{2} \right]\sigma_x^4 \\ & - \frac{1}{4}\left[\frac{3}{8}(\sigma_{yF}^4 + \sigma_{yA}^4) + \frac{1}{4}\sigma_{yA}^2\sigma_{yF}^2 \right] \\ & - \frac{1}{4}\left[\frac{3}{8}(\sigma_{zF}^4 + \sigma_{zA}^4) + \frac{1}{4}\sigma_{zA}^2\sigma_{zF}^2 \right]. \end{aligned} \tag{10}$$

Notice that in Eq. (10) the values of σ_{yF}, σ_{yA}, σ_{zF}, and σ_{zA}, given by Eq. (8), correspond to the equilibrium values if σ_x minimizes G. Therefore, the stability of the different competing magnetic phases can be simply determined by imposing the equilibrium condition $\frac{\partial G}{\partial \sigma_x} = 0$, together with the stability conditions $\frac{\partial^2 G}{\partial \sigma_i^2} > 0$ and $\det\left[\frac{\partial^2 G}{\partial \sigma_i \partial \sigma_j}\right] > 0$. For simplicity, we will consider only the potential stability of the phases that are experimentally observed. Consequently, we will ignore mixed phases where two or more of the secondary parameters σ_{yF}, σ_{yA}, σ_{zF}, and σ_{zA} coexist, or ferroelastic phases with nonzero σ_{zF} or σ_{yF}. We will focus on the competition between four relevant phases: the L-INC phase, the cycloidal polar phases corresponding to the order parameters σ_x and σ_{yA} ($\vec{P} \| \vec{b}$, Cycl-XY) or σ_x and σ_{zA} ($\vec{P} \| \vec{c}$, Cycl-XZ) and the homogeneous A-AFM phase.

1. Phase 1: The AFM phase ($\sigma_x \neq 0$ and $\sigma_y = \sigma_z = 0$)

The free energy corresponding to the homogeneous ($\vec{q} = 0$) antiferromagnetic phase is $G_1 = -t^2$ and the temperature dependence of the antiferromagnetic order parameter is $\sigma_x = \sqrt{-2t}$. This phase is potentially stable if $t < 0$.

2. Phase 2: The L-INC phase ($\sigma_x \neq 0$ and $\sigma_y = \sigma_z = 0$)

The free energy (G_2) and the amplitude of the magnetic modulation (σ_x) for this modulated phase ($\vec{q} \neq 0$) are given by

$$G_2 = -\frac{1}{4}\frac{\left[t - \frac{q^2}{4} + \frac{q^4}{4} \right]^2}{\left[\frac{3}{8} + \frac{1}{2}\mu q^2 \right]}, \tag{11a}$$

$$\sigma_x^2 = -\frac{\left[t - \frac{q^2}{4} + \frac{q^4}{4} \right]}{\left[\frac{3}{8} + \mu\frac{q^2}{2} \right]}. \tag{11b}$$

This phase will be stable if $\left[t - \frac{q^2}{4} + \frac{q^4}{4}\right] < 0$ (that is, $\sigma_x^2 > 0$). The temperature dependence of the incommensurate modulation wave vector, which can be obtained from the equilibrium condition $\frac{\partial G_2}{\partial q} = 0$, is given by the equation,

$$2q\left[t - \frac{q^2}{4} + \frac{q^4}{4} \right]\left\{ \left(q^2 - \frac{1}{2} \right)\left(\frac{3}{8} + \mu\frac{q^2}{2} \right) - \frac{\mu}{2}\left(t - \frac{q^2}{4} + \frac{q^4}{4} \right) \right\} = 0. \tag{11c}$$

The solutions $q = 0$ and $\left[t - \frac{q^2}{4} + \frac{q^4}{4}\right] = 0$ correspond to the nonmodulated antiferromagnetic phase and to the paramagnetic phase, respectively. The other solutions are

$$q_{\pm}^2 = \frac{1}{6\mu}\left\{ (\mu - 3) \pm 3\sqrt{1 + \frac{\mu^2}{9}(1 + 48t) + \frac{4}{3}\mu} \right\}. \tag{11d}$$

As can be seen from Eq. (11c), at the second-order transition point from the paramagnetic to the longitudinal incommensurate phase ($\sigma_x^2 \to 0$), these additional solutions correspond to $q_+^2 = \frac{1}{2}$ and $q_-^2 = -\frac{3}{4\mu}$. Since μ can be a positive constant, this latter solution must be discarded and the former one identified as that corresponding to the incommensurate phase. Then, from the condition $G_2(t_i) = 0$, one finds $t_i = \frac{1}{16}$. The experimental and reduced temperature and wave-vector scales are therefore related as

$$t = \frac{(T - T_0)}{16(T_i - T_0)},$$

$$q(t) = \frac{1}{\sqrt{2}}\frac{k(T)}{k(T_i)}, \tag{11e}$$

where T_i represents the experimental temperature of the zero magnetic field transition between the paramagnetic and the incommensurate phases.

3. Phase 3: The Cycl-XY phase ($\sigma_x \neq 0$ and $\sigma_{yA} \neq 0$; $\sigma_{zA} = \sigma_{zF} = \sigma_{yF} = 0$)

If, in addition to the primary longitudinal modulation $\sigma_x \neq 0$ there exists a secondary modulation of the y component

of the Mn spins that is in quadrature with σ_x, then the phase will develop, as seen, a spontaneous electrical polarization along the b axis given by $p_y=\nabla_2 q\sigma_x\sigma_{yA}$ while the ferroelastic deformation averages out. The energy of this ferroelectric phase is

$$G_3=-\frac{1}{4}\frac{\left[t-\frac{M}{4}q^2+\frac{1}{4}q^4\right]^2}{\left[\frac{3}{8}+\frac{\mu}{2}q^2-Nq^4\right]}-\frac{3}{8}\frac{[(t-t_1)]^2}{4}, \quad (12a)$$

where $M=1-\frac{3\nabla_2^2}{2}$ and $N=\frac{3\nabla_2^4}{8}$. The amplitude of the primary modulation and the stability conditions are, respectively, given by

$$\sigma_x^2=-\frac{\left[t-\frac{M}{4}q^2+\frac{1}{4}q^4\right]}{\left[\frac{3}{8}+\frac{\mu}{2}q^2-Nq^4\right]} \quad (12b)$$

and

$$\left[t-\frac{M}{4}q^2+\frac{1}{4}q^4\right]<0,$$

$$\left[\frac{3}{8}+\frac{\mu}{2}q^2-Nq^4\right]>0,$$

$$\nabla_2^2q^2\sigma_x^2>a_y(t-t_1). \quad (12c)$$

As before, the temperature dependence of the incommensurate modulation wave vector can be obtained from the equilibrium condition $\frac{\partial G_3}{\partial q}=0$. This leads to the equation,

$$2q\left[t-M\frac{q^2}{4}+\frac{q^4}{4}\right]\left\{\left(q^2-\frac{M}{2}\right)\left(\frac{3}{8}+\mu\frac{q^2}{2}-Nq^4\right)-\left(\frac{\mu}{2}-2Nq^2\right)\left(t-M\frac{q^2}{4}+\frac{q^4}{4}\right)\right\}=0 \quad (12d)$$

and to a temperature dependence of the cycloidal wave vector given by one real root of the equation,

$$-\frac{N}{2}q^6+\frac{3}{8}\mu q^4+\left(\frac{3}{8}-\frac{\mu M}{8}-2Nt\right)q^2+\left(\frac{3}{16}M-\frac{\mu t}{2}\right)=0. \quad (12e)$$

4. Phase 4: The Cycl-XZ phase ($\sigma_x\neq 0$ and $\sigma_{zA}\neq 0$; $\sigma_{zF}=\sigma_{yA}=\sigma_{yF}=0$)

This case is similar to the previous one but with the cycloid lying on the xz plane and the spontaneous polarization directed along the z axis ($p_z=\xi_2 q\sigma_x\sigma_{zA}$). The energy of this phase is given by

$$G_4=-\frac{1}{4}\frac{\left[t-\frac{M'}{4}q^2+\frac{1}{4}q^4\right]^2}{\left[\frac{3}{8}+\frac{\mu}{2}q^2-N'q^4\right]}-\frac{3}{8}\frac{[(t-t_2)]^2}{4}, \quad (13a)$$

where $M'=1-\frac{3\xi_2^2}{2}$ and $N'=\frac{3\xi_2^4}{8}$. The amplitude of the primary modulation and the stability conditions are, respectively, given by

$$\sigma_x^2=-\frac{\left[t-\frac{M'}{4}q^2+\frac{1}{4}q^4\right]}{\left[\frac{3}{8}+\frac{\mu}{2}q^2-N'q^4\right]} \quad (13b)$$

and

$$\left[t-\frac{M'}{4}q^2+\frac{1}{4}q^4\right]<0,$$

$$\left[\frac{3}{8}+\frac{\mu}{2}q^2-N'q^4\right]>0,$$

$$\xi_2^2q^2\sigma_x^2>(t-t_2). \quad (13c)$$

Finally, the equilibrium condition $\frac{\partial G_4}{\partial q}=0$ leads to the equation

$$-\frac{N'}{2}q^6+\frac{3}{8}\mu q^4+\left(\frac{3}{8}-\frac{\mu M'}{8}-2N't\right)q^2+\left(\frac{3}{16}M'-\frac{\mu t}{2}\right)=0, \quad (13d)$$

which can be solved in order to q to give the temperature dependence of the incommensurate modulation wave vector, common to both magnetic order parameters.

IV. MODELING THE PHASE DIAGRAMS OF THE RMnO$_3$ COMPOUNDS

As seen above, the crystalline distortion that leads to magnetic frustration and, eventually, to the ferroelectric order, mainly originates from the ionic radii of the rare-earth ions. This geometric effect can be controlled either in a stepwise manner, by using rare-earth elements with different ionic radius (from R=La^{3+} to Pr^{3+}, Eu^{3+}, Gd^{3+}, Tb^{3+}, Dy^{3+}, Ho^{3+}, Yb^{3+}, and Lu^{3+}), or quasicontinuously, by tuning the average rare-earth radius in solid solutions in which the R^{3+} ion is partially replaced by one isoelectric ion with different ionic radius, as in the case of the Eu$_{1-x}$Y$_x$MnO$_3$ mixed system.[14,61–63] In the following we will analyze these two cases within the scope of the model presented above, as illustrative examples.

A. Pure compounds

Figure 2 shows the experimental temperature dependence of the modulation wave vector in the Gd, Tb, Dy, and Ho compounds (dots; data taken from Ref. 25). As seen in the preceding section, the evolution of the modulation wave vector with temperature in the L-INC phase is solely deter-

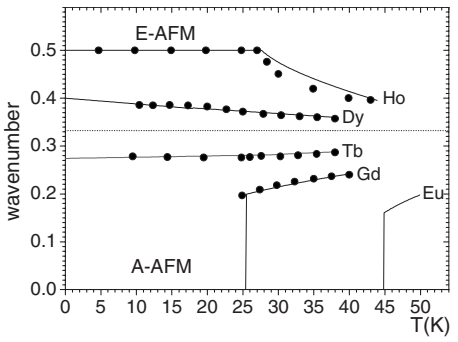

FIG. 2. (a) Experimental (dots) and simulated (lines) temperature dependences of the modulation wave numbers for the $R\mathrm{MnO_3}$ compounds (R=Gd, Tb, Dy, and Ho). For $\mathrm{EuMnO_3}$ only the simulation is shown (see text).

mined, in the model, by the signal and magnitude of the coupling constant μ, along with the value of T_0. For a given compound, these two constants can be estimated by fitting $q_+(t,\mu)$ given by Eq. (11d) to the experimental $\delta_{inc}(T)$ curve, and by taking into account that the relationship between the experimental and the reduced temperature and wavelength scales is given by Eq. (11e). The curves fitted to the experimental data in this way (see lines in Fig. 2) reproduce well the essential features of the observed behavior of the modulation wavenumber $\delta(T)$.

In the L-INC phase and on cooling, $\delta(T)$ decreases for Gd and Tb and increases for Dy and Ho. This behavior implies a transition from a positive to a negative μ, as the ionic radius R_{ion} decreases. As shown in Fig. 3(a) (see also Table III), μ varies almost linearly with the ionic radius of the rare-earth elements, from $\mu \sim 1$ for Gd to $\mu \sim -0.7$ for Ho. The value $\mu=0$, for which the modulation wavelength is independent of the temperature, can be estimated from the linear fit as $R \sim 105.7$ pm, a value that is intermediate between Tb (106.3 pm) and Dy (105.2 pm). Given the linear relationship between $\delta(T_i)$ and R_{ion}, this value would correspond to the commensurate value $\delta(T_i) \sim 1/3$. These conclusions are in excellent agreement with the behavior experimentally observed in the $\mathrm{Tb_{1-x}Dy_x\,MnO_3}$, where a spin modulation with a temperature independent wave number $\delta \sim \frac{1}{3}$ is observed for compositions in the range $0.5 < x < 0.68$ (Ref. 64).

The dependence of T_0 on the rare-earth ionic radius is not very pronounced for the Gd, Tb, Dy, and Ho compounds, varying only slightly within the range 32–36 K [see Fig. 3(b)]. It is interesting, however, to consider how this parameter varies outside this range of rare-earth elements. As seen, T_0 corresponds to the temperature for which the magnon branch softens at the center of the Brillouin zone. For compounds such as $\mathrm{LaMnO_3}$, $\mathrm{PrMnO_3}$, $\mathrm{NdMnO_3}$, and $\mathrm{SmMnO_3}$, for which frustration does not occur, T_0 corresponds to the critical temperature of the direct transition between the PM and the A-AFM phases. This implies that T_0 decreases rather steeply as R_{ion} decreases in the range 107 pm $< R_{ion} <$ 117 pm [see inset of Fig. 3(b)], stabilizing at a more or less constant values once magnetic frustration is achieved and the intermediate L-INC phase is induced (within the range from Eu to Ho).

For the case of $\mathrm{EuMnO_3}$ there are no reported data on the temperature dependence of $\delta(T)$ within the narrow temperature range of stability of the L-INC phase (50 K $< T <$ 46 K). However, from the linear dependence of μ and $\delta(T_i)$ on R_{ion}, one can estimate, for this compound (R_{ion} = 108.7 pm), the values $\mu=1.36$ and $\delta(T_i) \sim 0.19$. Then, if we adopt these values, we are left with a single parameter (T_0) to fit the critical temperature of the transition between the L-INC and the A-AFM phases. The fit of this unique parameter gives $T_0 \sim 48$ K, a value that is entirely consistent with the general trend of $T_0(R_{ion})$ seen in the inset of Fig. 3. In addition, the set of parameters thus found for the Eu compound [μ, T_0 and $\delta(T_i)$] allows us to estimate the function $\delta(T)$ within the L-INC phase. This estimated temperature dependence of the modulation wave number is depicted in Fig. 2.

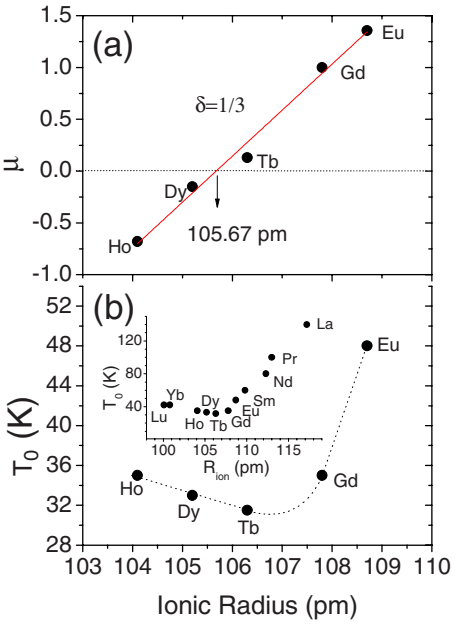

FIG. 3. (Color online) The dependence of the parameters (a) μ and (b) T_0 on the ionic radius of the rare-earth ion R (from Eu to Ho). The inset in (b) shows the variation in T_0 over an extended range that includes R=La, Sm Pr, Nd, Yb, and Lu (see text).

For the cases of the Tb and the Dy systems, the ground state is the cycloidal modulated phase (Cycl-XY), which is polar ($\vec{P} \| \vec{b}$). Here, we have to include the analysis of the potential stability of this additional phase and tune the additional parameters ∇_2 and T_1 in order to account for both the observed transition temperature from the L-INC to the

TABLE III. The values of the model parameters μ, ∇_2, T_0, and T_1 that allow the simulation of the phase-transition sequences observed experimentally. The values of T_{inc} and $\delta(T_i)$ are also given.

	μ	∇_2	T_0	T_1	T_{inc}	$\delta(T_i)$
$\mathrm{EuMnO_3}$	1.35		48		50	0.198
$\mathrm{GdMnO_3}$	1		35		40	0.242
$\mathrm{TbMnO_3}$	0.2	0.6	31.5	24	38	0.288
$\mathrm{DyMnO_3}$	−0.15	0.3	33	15	38	0.36
$\mathrm{HoMnO_3}$	−0.68		35		44	0.395

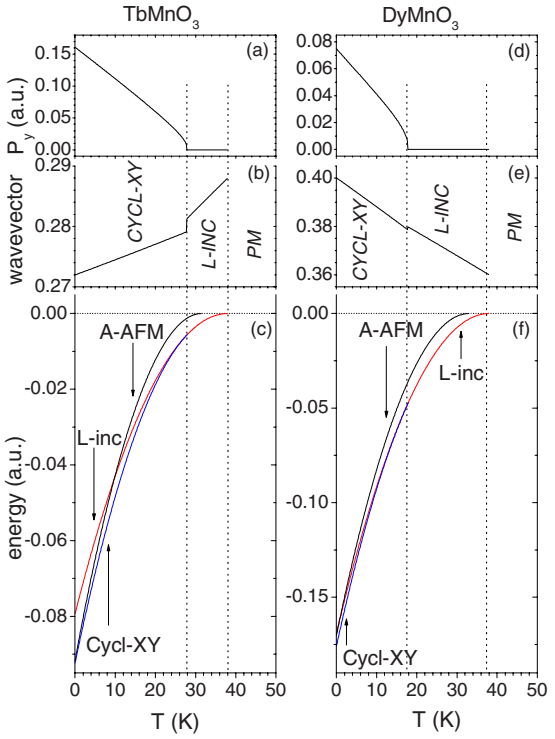

FIG. 4. (Color online) Polarization, modulation wave vector, and free energy of the phases L-INC, Cycl-XY, and *A*-AFM as functions of temperature for [(a)–(c)] $TbMnO_3$ and [(d)–(f)] $DyMnO_3$. The model parameters are given in Table III and the reference energy corresponds to that of the paramagnetic phase.

Cycl-XY phase and the temperature dependence of the modulation wave vector in the range of stability of this lower temperature phase. As seen in Fig. 4, the values given in Table III for these additional parameters allow the simulation of the phase sequence PM→L-INC→Cycl-XY observed in these compounds at zero magnetic field. It is also possible to calculate the temperature dependence of both the electric polarization and the modulation wave vector near the transition from the L-INC to the Cycl-XY phase. These quantities are also plotted in Fig. 4 for these two intermediate compounds.

B. Solid solutions: The example of $Eu_{1-x}Y_xMnO_3$

The model can also be applied to the description of the phase diagrams of solid solutions in which the average value of the radius of the rare-earth element is tuned by the partial substitution of isoelectric ions. Here, we will analyze, as one illustrative example, the case of the $Eu_{1-x}Y_xMnO_3$ mixed system.

In the $Eu_{1-x}Y_xMnO_3$ solid solution, the *Pnma* orthorhombic symmetry is maintained only for $x<0.6$. Above this concentration, traces of the *P*63*cm* hexagonal phase of $YMnO_3$ appear. As x increases, the volume and the orthorhombic distortion of the unit cell cross the values found in $GdMnO_3$ ($x\sim0.2$) and $TbMnO_3$ ($x\sim0.8$). Despite the continuous shrinking of the lattice volume, the in-plane orthorhombic distortion, parameterized by $\varepsilon=(a-c)/(c+a)$, tends to saturate near $x\sim0.4$ (Ref. 14). Notice that the inequality of the lattice constants a and c reflects the tilting of the oxygen octahedral around the b axis and the consequent reduction in Mn-O-Mn bond angle. It is likely that this reduction may not be the only factor affecting the spin system. The shrinkage of the unit cell and the *A*-site disorder may also affect the orbital overlap and the magnetic exchange.

In the composition range $0<x<0.5$, the (x-T) diagram of the solid solution has been investigated by different groups.[14,61,62] The temperature range of stability of the L-INC phase increases from 51 K$>T>$46 K at $x=0$ to 45 K$>T>$22 K at $x=0.5$. For $x<0.2$, the *A*-AFM phase is stabilized at low temperatures, although within a temperature band that rapidly narrows as x decreases. For $x>0.3$ the *A*-AFM phase is suppressed and the low-temperature phase corresponds to a $P\|z$ ferroelectric phase. For $x=0.2$ the canted ferromagnetism ($M\|y$) characteristic of the *A*-AFM coexists, at low temperatures, with the $P\|z$ polarization.[14] This coexistence may signal either the stabilization of a more complex magnetic phase[14] or a coexistence of both phases. Although there is no direct experimental evidence, the $P\|z$ phase is attributed to the stabilization of the Cycl-XZ phase,[60] as observed in $GdMnO_3$ under a magnetic field.

In principle, for a solid solution, one can find the adequate model parameters by following the procedure described above for the case of the pure systems. That is, one can fit, for each composition, the transition temperatures and the temperature dependences of the modulation wave vectors within the ranges of stability of the different phases observed. Quite often, complete experimental information is not available but, for $Eu_{1-x}Y_x$ MnO_3, it exists at least in part.

The experimental temperature dependence of the magnetic modulation wave number $\delta(T)$ is shown in Fig. 5 for the compositions $x=0.2$, $x=0.3$, and $x=0.4$ (Ref. 62). The curve predicted for $EuMnO_3$ (see above) is also shown for comparison. For a given composition, the model parameters can be fit in order to simultaneously reproduce $\delta(x,T)$ and the temperature ranges of stability of the phases observed. For the three compositions shown, the values of the model parameters obtained in this way are listed in Table IV. Notice that the parameters μ and T_0 can be determined for the three compositions because the L-INC phase is always stable. However, for $x=0.3$, the wave number corresponding to the Cycl-XZ phase locks at the commensurate value $\delta=\frac{1}{4}$. Therefore, only in the case of $x=0.4$, where both the incommensurate Cycl-XY and Cycl-XZ are stable, can one explicitly determine the values of ∇_2, ξ_2, T_1, and T_2. This has been done by carefully fitting, for this composition, the temperature ranges of stability of the two cycloidal phases and the experimental temperature dependence of the modulation wave number [see Fig. 6(a)]. The parameters adjusted is this way allow us to calculate the temperature dependence of the electrical polarizations P_y and P_z and to describe the polarization rotation observed at the transition between the Cycl-XY and the Cycl-XZ phases [Fig. 6(b)]. Due to the limited experimental information, we have decided to maintain, for the other compositions, the values of ∇_2, ξ_2, and T_1 as determined for $x=0.4$.

As seen above, the cycloidal-XZ spin modulation observed for $x=0.3$ is commensurate ($\delta=1/4$). In an incommensurate phase, we consider the modulation wave number as a variational parameter whose value, at equilibrium, results from the condition $\frac{\partial G}{\partial q}=0$.

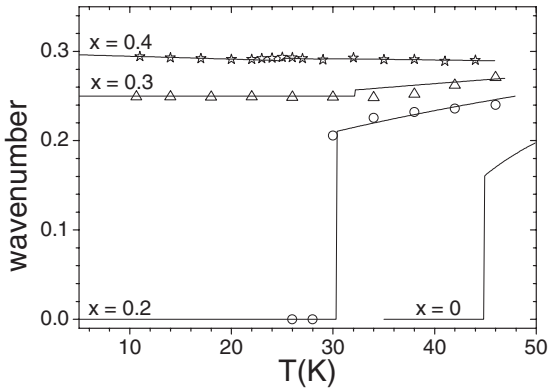

FIG. 5. Experimental (dots) and simulated (lines) of the temperature dependence of the wave numbers of the magnetic modulation in the $Eu_{1-x}Y_x$ MnO_3 mixed system for the compositions $x=0.2$, $x=0.3$, and $x=0.4$. The experimental data was taken from Ref. 62. The predicted modulation wave number for pure $EuMnO_3$ is also shown for comparison.

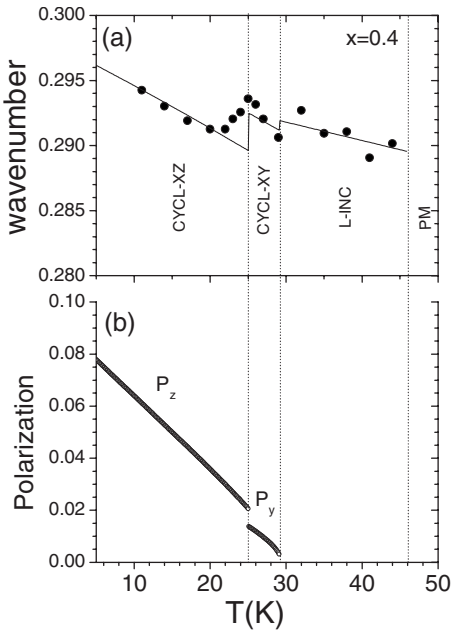

FIG. 6. (a) Detail of the experimental (dots) and fitted (line) temperature dependence of the modulation wave number of the spin wave for $x=0.4$; (b) the electric polarizations P_y and P_z as functions of the temperature. The polarization rotation observed at the transition between the Cycl-XY and the Cycl-XZ phases is well reproduced by the model.

However, a given commensurate phase has a fixed rational modulation wave number $\delta=\frac{n}{p}$. In general, this fixed value of δ costs energy, when compared to the incommensurate solution considered above. This cost may be compensated by the additional terms (umklapp invariants) that are, in this case, allowed by symmetry. These umklapp terms are of degree $2p$ $(p>2)$ for a commensurate wave number $\delta=\frac{n}{p}$ (n and p integers). In the case of the $\delta=1/4$ cycloidal phase observed for $x=0.3$, we have assumed, for simplicity, that the effect of the lock-in potential $U_{umklapp}=-\beta\sigma_x^8$ could be described by means of effective fourth degree terms in the primary order-parameter amplitude $(U_{umklapp}\approx\frac{1}{4}\beta_{eff}\sigma_x^4)$. This approximation can be justified by the fact that the $\delta=1/4$ phase is observed in a temperature range well below T_i, implying that the temperature dependence of the amplitude of the order parameter σ_x is already weak $[\sigma_x\sim(T-T_i)^{1/2}]$. Consequently, the temperature dependence of β_{eff} is not important and can be neglected. In other words, it is not the degree of the lock-in term but rather its presence and magnitude that modify the free energy. In this approximation, the energy of the $\delta=1/4$ phase can be estimated by replacing in the incommensurate free energy $q(t)=\frac{1}{\sqrt{2}}\frac{\delta(T)}{\delta(T_i)}$ by $q_c=\frac{1}{\sqrt{2}}\frac{1/4}{\delta(T_i)}$ and by adding the contribution of the effective lock-in potential averaged over a period of the modulation wave, $U=-\frac{3}{8}(\frac{1}{4}\beta_{eff}\sigma_x^4)$. For $x=0.3$, we have used in the simulation the minimum value of β_{eff} required to stabilize the commensurate phase and the value of T_2 necessary to fit the observed transition temperature ($\beta_{eff}=0.003$). We have maintained this value of β_{eff} to estimate the free energy of the $\delta=1/4$ phase for all the other compositions.

Under these circumstances, for any given value of x within the range $0<x<0.5$, the values of the parameters μ, T_0, $T_{\rm inc}$, and $\delta(T_i)$ can be interpolated by polynomial fitting. By doing so, we maintain a single adjustable parameter (T_2) to model the observed (T,x) phase diagram of the solid solution. Notice that the value of T_2 solely influences the range of stability of the Cycl-XZ phase and the temperature dependence of the modulation wave number within this phase. As seen in Fig. 7, the experimental phase diagram taken from Ref. 14 can be very well reproduced if one assumes that T_2 decreases smoothly with x as illustrated in the inset of the figure.

V. CONCLUDING REMARKS

The present paper described one unified Landau model for the phase diagrams of the rare-earth orthomanganese com-

TABLE IV. The values of the model parameters μ, ∇_2, ξ_2 T_0, T_1, and T_2 allowing the simulation of the (T-x) dependence of the modulation wave vector and of the phase-transition sequences observed experimentally in the three compositions. The experimental values of $T_{\rm inc}$ and $\delta(T_i)$ are also given. The $\beta_{eff}(1/4)$ coefficient corresponds to the effective lock-in potential to the C phase with $\delta=1/4$.

	μ	∇_2	ξ_2	T_0	T_1	T_2	$T_{\rm inc}$	$\delta(T_i)$	$\beta_{eff}(1/4)$
$EuMnO_3$	1.35			48			50	0.198	0.003
$Eu_{0.8}Y_{0.2}$ MnO_3	1.04	0.5	0.7	38.68	23.5	25.85	48	0.243	0.003
$Eu_{0.7}Y_{0.3}$ MnO_3	0.59	0.5	0.7	35.47	23.5	23.03	47	0.266	0.003
$Eu_{0.6}Y_{0.4}$ MnO_3	−0.04	0.5	0.7	33.26	23.5	17	46	0.290	0.003

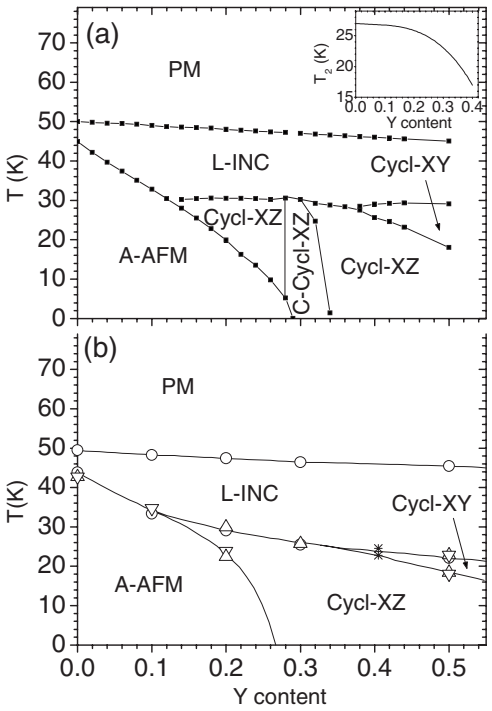

FIG. 7. (a) Simulated and (b) experimental temperature versus composition phase diagram of the $Eu_{1-x}Y_x$ MnO_3 solid solution. The experimental phase diagram was taken from Ref. 14. The inset shows the concentration dependence of the adjustable parameter T_2 (see text).

pounds. The common symmetry $\Gamma(B_2)$ of the primary magnetic order parameters over the whole set of the orthorhombic $R\mathrm{MnO_3}$ compounds was stressed and used to obtain, in the simplest possible terms, an unified phenomenological description of the phase-transition sequences observed. Besides the primary parameter, the model also includes two additional magnetic modes of symmetry $\Gamma(A_2)$ and $\Gamma(A_1)$, which couple biquadratically to the primary mode. This set of three active magnetic modes of distinct symmetries can be related to the softening of the three spatial components of the $\vec{A}$ basis mode of the Mn^{3+} spins. As in the case of typical displacive modulated systems, the type-II Landau description of modulated phases was used to generate adequate free-energy functionals for the different competing phases.

The model is rooted in exact-symmetry considerations. This fact guarantees the consistency of the overall picture and elucidates the possible coupling between the different degrees of freedom. In particular, the potential ferroelectric and ferroelastic properties of a given magnetic phase can be clearly established, either by searching for the allowed mixed invariants that are linear on a particular electric polarization or lattice deformation, or by establishing, directly, the magnetic symmetry of the ordered phase.

The model is capable of generating the observed phase diagrams and account for the polar properties of a given compound or solid solution. However, magnetoelectric biferroicity and ferromagnetoelectricity (the linear magnetoelectric effect) are here entirely excluded by symmetry. That is, the phases considered in the present model (and observed experimentally in these compounds at zero magnetic field) may be improper ferroelectric phases but are not multiferroic phases, at least if the standard notion of ferroic order is adopted. Notice, for example, that the phase transitions observed in $TbMnO_3$ corresponds, on cooling, to the sequence $(Pnma)' \rightarrow P_a(P^{nma}_{\bar{1}1S}) \rightarrow P_a(P^{n2_11^a}_{\bar{1}1S})$. This last phase, $P_a(P^{n2_11^a}_{\bar{1}1S})$, is ferroelectric $(\vec{P}\|\vec{b})$ but it is neither ferromagnetoelectric nor multiferroic. Also, the thermally induced polarization rotation observed in $Eu_{0.5}Y_{0.5}$ MnO_3 corresponds to a phase transition involving the cycloidal phases Cycl-XY $[(P_a(P^{n2_11^a}_{\bar{1}SS}), \vec{P}\|\vec{b}]$ and Cycl-XZ $[(P_a(P^{nm2_1}_{\bar{1}SS}), \vec{P}\|\vec{c}]$ which, once again, have symmetries that are incompatible with ferromagnetoelectricity or multiferroicity.

[1] J. C. Tolédano and P. Tolédano, *The Landau Theory of Phase Transitions* (World Scientific, Singapore, 1987).

[2] T. Kimura, T. Goto, H. Shintani, K. Ishizaka, T. Arima, and Y. Tokura, Nature (London) **426**, 55 (2003).

[3] N. Hur, S. Park, P. A. Sharma, J. S. Ahn, S. Guha, and S. W. Cheong, Nature (London) **429**, 392 (2004).

[4] G. Lawes, A. B. Harris, T. Kimura, N. Rogado, R. J. Cava, A. Aharony, O. Entin-Wohlman, T. Yildrim, M. Kenzelmann, C. Broholm, and A. P. Ramirez, Phys. Rev. Lett. **95**, 087205 (2005).

[5] T. Kimura, J. C. Lashley, and A. P. Ramirez, Phys. Rev. B **73** 220401(R) (2006).

[6] Y. Yamasaki, S. Miyasaka, Y. Kaneko, J. P. He, T. Arima, and Y. Tokura, Phys. Rev. Lett. **96**, 207204 (2006).

[7] K. Taniguchi, N. Abe, T. Takenobu, Y. Iwasa, and T. Arima, Phys. Rev. Lett. **97**, 097203 (2006).

[8] O. Heyer, N. Hollmann, I. Klassen, S. Jodlank, L. Bohatý, P. Becker, J. A. Mydosh, T. Lorenz, and D. Khomskii, J. Phys.: Condens. Matter **18**, L471 (2006).

[9] T. Kimura, G. Lawes, and A. P. Ramirez, Phys. Rev. Lett. **94**, 137201 (2005).

[10] S. W. Cheong and M. Mostovoy, Nature Mater. **6**, 13 (2007).

[11] J. R. Teague, R. Gerson, and W. J. James, Solid State Commun. **8**, 1073 (1970).

[12] E. F. Bertaut, in *Magnetism*, edited by G. T. Rado and H. Suhl (Academic Press, New York, 1963), Vol. III, p. 149.

[13] T. Kimura, S. Kawamoto, I. Yamada, M. Azuma, M. Takano, and Y. Tokura, Phys. Rev. B **67**, 180401 (2003).

[14] J. Hemberger, F. Schrettle, A. Pimenov, P. Lunkenheimer, V. Y. Ivanov, A. A. Mukhin, A. M. Balbashov, and A. Loidl, Phys. Rev. B **75**, 035118 (2007).

[15] Y. Yamasaki, H. Sagayama, N. Abe, T. Arima, K. Sasai, M. Matsuura, K. Hirota, D. Okuyama, Y. Noda, and Y. Tokura, Phys. Rev. Lett. **101**, 097204 (2008).

[16] I. A. Sergienko, C. Sen, and E. Dagotto, Phys. Rev. Lett. **97**, 227204 (2006).

[17] I. A. Sergienko and E. Dagotto, Phys. Rev. B **73**, 094434 (2006).

[18] A. D. Bruce, R. A. Cowley, and A. F. Murray, J. Phys. C **11**,

3591 (1978).
[19] V. N. Krivoruchko and T. E. Prymak, Low Temp. Phys. **29**, 294 (2003).
[20] F. Zhong and Z. D. Wang, Phys. Rev. B **60**, 11883 (1999).
[21] G. C. Milward, M. J. Calderón, and P. B. Littlewood, Nature (London) **433**, 607 (2005).
[22] *Physics of Manganites*, edited by T. Kaplan and S. D. Mahanti (Plenum, New York, 1999).
[23] We will adopt the *Pnma* setting, which is the standard, as opposed to the *Pbnm* setting used by some authors.
[24] Here, the magnetic symmetry is described by the unitary space group $P1\frac{2_1}{m}1$ plus nonunitary operations (θC_{2x}, θC_{2z}, $\theta\sigma_x$, and $\theta\sigma_z$) that recover a *Pnma* symmetry.
[25] T. Kimura, S. Ishihara, H. Shintani, T. Arima, K. T. Takahashi, K. Ishizaka, and Y. Tokura, Phys. Rev. B **68**, 060403(R) (2003).
[26] E. Dagotto, *Nanoscale Phase Separation and Colossal Magnetoresistence* (Springer, Berlin, 2002).
[27] T. Goto, T. Kimura, G. Lawes, A. P. Ramirez, and Y. Tokura, Phys. Rev. Lett. **92**, 257201 (2004).
[28] T. Kimura, G. Lawes, T. Goto, Y. Tokura, and A. P. Ramirez, Phys. Rev. B **71**, 224425 (2005).
[29] M. Kenzelmann, A. B. Harris, S. Jonas, C. Broholm, J. Schefer, S. B. Kim, C. L. Zhang, S. W. Cheong, O. P. Vajk, and J. W. Lynn, Phys. Rev. Lett. **95**, 087206 (2005).
[30] A. B. Harris, Phys. Rev. B **76**, 054447 (2007); **77**, 019901(E) (2008).
[31] A. B. Harris, A. Aharony, and O. Entin-Wohlmann, J. Phys.: Condens. Matter **20**, 434202 (2008).
[32] J. L. Ribeiro, Phys. Rev. B **76**, 144417 (2007).
[33] J. L. Ribeiro, J. Phys.: Conf. Ser. **226**, 012013 (2010).
[34] $P_a(P^{nma}_{\bar{1}1S})$ denotes $P^{nma}_{\bar{1}1S}\otimes[\{E;000,0\},\{\theta;000,1/2\}]$, where $P^{nma}_{\bar{1}1S}$ is the unitary superspace group (in the standard notation).
[35] H. W. Brinks, J. Rodríguez-Carvajal, H. Fjellväg, A. Kjekshus, and B. C. Hauback, Phys. Rev. B **63**, 094411 (2001).
[36] For Ho-Lu, Y, and Sc, the lower energy structure becomes a layerlike structure with hexagonal symmetry ($P6_3cm$). However, even in this range of smaller ions, high-pressure techniques, low soft chemistry, or epitaxial thin-film growth still allow the synthesis of orthorhombic compounds.
[37] H. Okamoto, N. Imamura, B. C. Hauback, M. Karppinen, H. Yamauchi, and H. Fjellvag, Solid State Commun. **146**, 152 (2008).
[38] Y. H. Huang, H. Fjellvag, M. Karppinen, B. C. Hauback, H. Yamauchi, and J. B. Goodenough, Chem. Mater. **18**, 2130 (2006).
[39] A. Muñoz, M. T. Casáis, J. A. Alonso, M. J. Martínez-Lope, J. L. Martínez, and M. T. Fernández-Díaz, Inorg. Chem. **40**, 1020 (2001).
[40] J.-S. Zhou and J. B. Goodenough, Phys. Rev. Lett. **96**, 247202 (2006).
[41] B. Lorenz, Y. Q. Wang, and C. W. Chu, Phys. Rev. B **76**, 104405 (2007).
[42] J. L. García-Muñoz, J. Rodríguez-Carvajal, and P. Lacorre, Phys. Rev. B **50**, 978 (1994).
[43] J. A. Alonso, J. L. García-Muñoz, M. T. Fernández-Díaz, M. A. G. Aranda, M. J. Martinez-Lope, and M. T. Casais, Phys. Rev. Lett. **82**, 3871 (1999).
[44] M. T. Fernández-Díaz, J. A. Alonso, M. J. Martínez-Lope, M. T. Casais, and J. L. García-Muñoz, Phys. Rev. B **64**, 144417 (2001).
[45] J.-S. Zhou, J. B. Goodenough, and B. Dabrowski, Phys. Rev. Lett. **95**, 127204 (2005).
[46] I. Dzyaloshinsky, J. Phys. Chem. Solids **4**, 241 (1958).
[47] T. Moriya, Phys. Rev. **120**, 91 (1960).
[48] H. Katsura, N. Nagaosa, and A. V. Balatsky, Phys. Rev. Lett. **95**, 057205 (2005).
[49] J. Hu, Phys. Rev. Lett. **100**, 077202 (2008).
[50] M. Mostovoy, Phys. Rev. Lett. **96**, 067601 (2006).
[51] N. Aliouane, K. Schmalzl, D. Senff, A. Maljuk, K. Prokes, M. Braden, and D. N. Argyriou, Phys. Rev. Lett. **102**, 207205 (2009).
[52] L. D. Landau and E. M. Lifshitz, *Statistical Physics* (Pergamon, New York, 1968).
[53] A. P. Levanyuk and D. G. Sannikov, Fiz. Tverd. Tela (Leningrad) **18** 1927 (1976) [Sov. Phys. Solid State **18**, 1122 (1976)]; D. G. Sannikov, Fiz. Tverd. Tela (Leningrad) **23**, 3140 (1981) [Sov. Phys. Solid State **23**, 1827 (1981)].
[54] P. Lederer and C. M. Chaves, J. Phys. (Paris) Lett. **42**, L127 (1981).
[55] J. L. Ribeiro, J. C. Tolédano, M. R. Chaves, A. Almeida, H. E. Muser, J. Albers, and A. Klopperpieper, Phys. Rev. B **41**, 2343 (1990).
[56] The bilinear terms coupling A_x to the pseudoproper order parameters F_y and G_z, although allowed by the symmetry (see Table I), were not included in f_1 because these pseudoproper distortions do not modify the symmetry constraints imposed on the secondary modes. Their inclusion is therefore irrelevant for the present analysis. Similarly, the bilinear terms coupling A_y with F_x and C_z and A_z with G_x and C_y will not be taken into account in the free-energy density f_2.
[57] If one considers an external magnetic field B, additional terms $[\delta A_x^2+\lambda_1 A_y^2+\lambda_2 A_z^2+(2\chi_m)^{-1}]M^2-MB$ must be considered, where M is the induced magnetization. In this work, however, we will consider only the case $B=0$.
[58] P. Tolédano, Phys. Rev. B **79**, 094416 (2009).
[59] P. Tolédano, W. Schranz, and G. Krexner, Phys. Rev. B **79**, 144103 (2009).
[60] We have checked, by numerical simulation, that significant distortions of the phase diagrams are only generated when these parameters differ from unity more than one order of magnitude.
[61] K. Noda, M. Akaki, T. Kikuchi, D. Akahoshi, and H. Kuwahara, J. Appl. Phys. **99**, 08S905 (2006).
[62] Y. Yamasaki, S. Miyasaka, T. Goto, H. Sagayama, T. Arima, and Y. Tokura, Phys. Rev. B **76**, 184418 (2007).
[63] M. Tokunaga, Y. Yamasaki, Y. Onose, M. Mochizuki, N. Furukawa, and Y. Tokura, Phys. Rev. Lett. **103**, 187202 (2009).
[64] T. Arima, A. Tokunaga, T. Goto, H. Kimura, Y. Noda, and Y. Tokura, Phys. Rev. Lett. **96**, 097202 (2006).